

EXPERIMENTAL AND ANALYTICAL EVALUATION OF LATERAL BUCKLING OF FRP COMPOSITE CANTILEVER I-BEAMS

*Pizhong Qiao and Guiping Zou, The University of Akron, Akron, OH
Julio F. Davalos, West Virginia University, Morgantown, WV*

Abstract

Pultruded Fiber-reinforced plastic (FRP) shapes (beams and column) are thin-walled or moderately thick-walled open or closed sections consisting of assemblies of flat panels. Due to the high strength-to-stiffness ratio of composites and thin-walled sectional geometry of FRP shapes, buckling is the most likely mode of failure before material failure for FRP shapes. In this paper, a combined analytical and experimental approach is used to characterize the lateral buckling of pultruded FRP composite cantilever I-beams. An energy method based on nonlinear plate theory is developed, and it includes shear effects and bending-twisting coupling. Three types of buckling mode shape functions (exact transcendental function, polynomial function, and half simply-supported beam function), which all satisfy the cantilever beam boundary conditions, are used to derive the critical buckling loads, and the accuracy of these approximations are studied and discussed. The effects of tip-load position, fiber orientation and fiber volume fraction on the critical buckling loads are investigated. Four common FRP I-beams with different cross-sectional geometries and various span lengths are experimentally tested, and the critical buckling loads are measured. A good agreement among the proposed analytical method, experimental testing and finite-element modeling is observed, and simplified explicit equations for lateral buckling of cantilever I-beams with the applied load at the centroid of the cross-section are formulated. The proposed analytical solution can be used to predict the lateral buckling loads for FRP cantilever I-beams and to assist practitioners to perform buckling analyses of customized FRP shapes as well as to optimize innovative sections.

Keywords: FRP Structural Shapes; Lateral Buckling; Cantilever Beams.

Introduction

Fiber-reinforced plastic (FRP) structural shapes (beams and columns) have shown to provide efficient and economical applications for civil engineering construction (e.g., in bridges, piers, retaining walls, airport facilities, storage structures exposed to salts and chemicals, and others). Most FRP shapes are thin-walled structures and manufactured by the pultrusion process. The material constituents for low-cost pultruded FRP shapes commonly consist of high-strength E-glass fiber and vinylester or polyester polymer resins, and due to this choice of materials, the structures usually exhibit relatively large deformations and tend to buckle globally or locally. Consequently, buckling is the most likely mode of failure before the ultimate load reaches the material failure [1-4].

A long slender beam under bending about the strong axis may buckle by a combined twisting and lateral (sideways) bending of the cross section. This phenomenon is known as lateral buckling, and an extensive review of analytical and theoretical investigations for steel and FRP composite beams has been presented in [5]. In this paper, a combined analytical and experimental study on lateral buckling of FRP cantilever I-beams is presented, and simplified equations for lateral buckling analysis are developed. Three different types of shape functions (exact transcendental function, polynomial

function, and half simply-supported beam function), which all satisfy the cantilever beam boundary conditions, are used to obtain eigenvalue solutions, and their numerical results are compared and discussed. The position of applied load through the cross section at the loading tip is also considered in the formulation. Four different geometries of FRP I-beams with varying span lengths are tested under tip loadings and cantilevered restrained at the other ends. The analytical solutions are compared with finite element studies and experimental tests. Parametric studies are further performed to study the fiber angle and fiber volume fraction effects on the lateral buckling behavior.

Brief Review of Analytical Formulation

The analysis of lateral buckling is based on total potential energy governing instability and derived using the plate theory [5]. In this section, a brief review of analytical formulation is presented, and the selection of buckling mode shape functions which are important to derive the accurate explicit solutions is introduced in details. The total potential energy for a plate structure under external force P is

$$\Pi = U + W = \frac{1}{2} \iiint_{\Omega} \sigma_{ij} \varepsilon_{ij} d\Omega - \sum_k P_k q_k \quad (1)$$

where P_k are the externally applied forces and q_k are the corresponding displacements. For an I-shape section, the strain energy includes the ones stored in two flanges and one web. The instability state is characterized by the vanishing of the second variation of the total potential energy [1, 5]

$$\delta^2 \Pi = \iiint_{\Omega} (\sigma_{ij} \delta^2 \varepsilon_{ij} + \frac{1}{2} \delta \sigma_{ij} \delta \varepsilon_{ij}) d\Omega - \sum_k P_k \delta^2 q_k = 0 \quad (2)$$

Also, since q_k can usually be expressed as linear functions of displacement variables, $\delta^2 q_k$ vanishes and $\sum_k P_k \delta^2 q_k$ can be omitted in Eq. (2). Because the displacement-gradient components are not small compared with unity, the strains for the buckling problem are expressed in nonlinear terms [5].

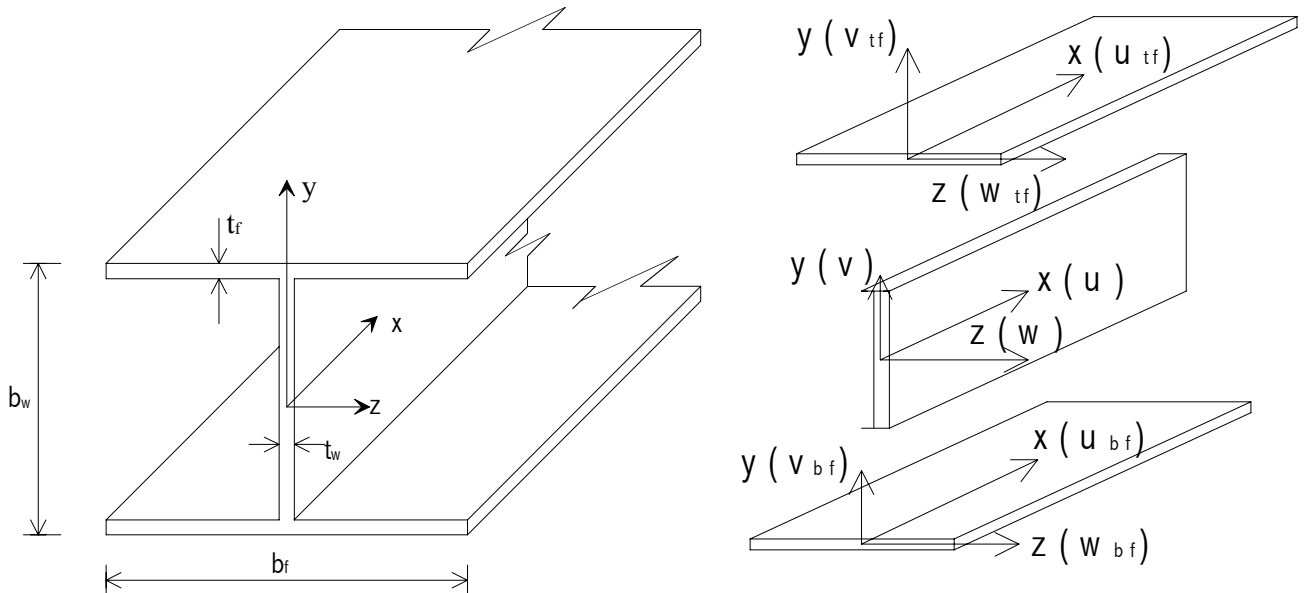


Figure 1. Coordinate system and geometry of I-beam

For buckling analysis of I-beams under bending, the deformation before buckling is ignored. Based on the coordinate system shown in Fig. 1, the buckled displacement fields are expressed as follows [5]:

$$u^w = 0, v^w = 0, w^w = w^w(x, y) \text{ for the web (in the } xy\text{-plane)} \quad (3a)$$

$$u^{TF} = u^{TF}(x, z), v^{TF} = v^{TF}(x, z), w^{TF} = w^{TF}(x) \text{ for the top flange (in the } xz\text{-plane)} \quad (3b)$$

$$u^{BF} = u^{BF}(x, z), v^{BF} = v^{BF}(x, z), w^{BF} = w^{BF}(x) \text{ for the bottom flange (in the } xz\text{-plane)} \quad (3c)$$

where the superscripts TF, W and BF refer to top flange, web, and bottom flange, respectively.

Considering the top and bottom flanges that can bend and twist as a plate and also bend laterally as a beam and also neglecting the transverse resultant forces, then the second variation of the total strain energy of the top and bottom flanges can be expressed as [5]

$$\begin{aligned} \delta^2 U^{TF} = & \frac{1}{2} \iint \left\{ N_x^{TF} \left[\left(\frac{\partial \delta v^{TF}}{\partial x} \right)^2 + \left(\frac{\partial \delta w^{TF}}{\partial x} \right)^2 \right] + \frac{1}{\alpha_{11}} \left(\frac{\partial \delta u^{TF}}{\partial x} \right)^2 \right. \\ & \left. + \frac{1}{\delta_{11}} \left(\frac{\partial^2 \delta v^{TF}}{\partial x^2} \right)^2 + \frac{4}{\delta_{66}} \left(\frac{\partial^2 \delta v^{TF}}{\partial x \partial z} \right)^2 \right\} dx dz \end{aligned} \quad (4a)$$

$$\begin{aligned} \delta^2 U^{BF} = & \frac{1}{2} \iint \left\{ N_x^{BF} \left[\left(\frac{\partial \delta v^{BF}}{\partial x} \right)^2 + \left(\frac{\partial \delta w^{BF}}{\partial x} \right)^2 \right] + \frac{1}{\alpha_{11}} \left(\frac{\partial \delta u^{BF}}{\partial x} \right)^2 \right. \\ & \left. + \frac{1}{\delta_{11}} \left(\frac{\partial^2 \delta v^{BF}}{\partial x^2} \right)^2 + \frac{4}{\delta_{66}} \left(\frac{\partial^2 \delta v^{BF}}{\partial x \partial z} \right)^2 \right\} dx dz \end{aligned} \quad (4b)$$

Similarly, considering the web as a plate, the second variation of the total strain energy of the web panel is expressed as

$$\begin{aligned} \delta^2 U^w = & \frac{1}{2} \iint \left[N_x^w \left(\frac{\partial \delta w^w}{\partial x} \right)^2 + N_y^w \left(\frac{\partial \delta w^w}{\partial y} \right)^2 + 2N_{xy}^w \frac{\partial \delta w^w}{\partial x} \frac{\partial \delta w^w}{\partial y} \right] dx dy \\ & + \frac{1}{2} \iint \left[D_{11}^w \left(\frac{\partial^2 \delta w^w}{\partial x^2} \right)^2 + D_{22}^w \left(\frac{\partial^2 \delta w^w}{\partial y^2} \right)^2 \right. \\ & \left. + 2D_{12}^w \frac{\partial^2 \delta w^w}{\partial x^2} \frac{\partial^2 \delta w^w}{\partial y^2} + 4D_{66}^w \left(\frac{\partial^2 \delta w^w}{\partial x \partial y} \right)^2 \right] dx dy \end{aligned} \quad (4c)$$

The buckling equilibrium equation $\delta^2 U = 0$ in terms of the lateral potential energy is then solved by the Rayleigh-Ritz method.

For a cantilever beam subjected to a tip concentrated vertical load, simplified stress resultant distributions on the corresponding panel are obtained from beam theory, and the location or height of the applied load is accounted for in the analysis. For FRP I-beams of uniform thickness, the membrane forces are expressed in terms of the tip applied concentrated load P . The expressions for the flanges are

$$\begin{aligned} N_x^{TF} &= \frac{b^w t^f}{2I} P(L-x) \\ N_z^{TF} &= N_{xz}^{TF} = 0 \end{aligned} \quad (5a)$$

$$N_x^{BF} = -\frac{b^w t^f}{2I} P(L-x) \quad (5b)$$

$$N_z^{BF} = N_{xz}^{BF} = 0$$

Similarly for the web

$$N_x^W = \frac{t^w}{I} P(L-x)y \quad (5c)$$

$$N_{xy}^W = -\frac{Pt^w}{2I} \left[\left(\frac{b^w}{2} \right)^2 - y^2 \right]$$

The transverse normal stress resultant (N_y^W) away from the concentrated load is zero. Denoting y_p as the distance from the centroidal axis to the location of the applied load, the transverse normal stress near the concentrated load, for the case of $y \neq \pm \frac{b^w}{2}$, is

$$N_y^W = P \frac{y + b^w/2}{y_p + b^w/2} \quad -b^w/2 \leq y \leq y_p \quad (5d)$$

$$N_y^W = P \frac{b^w/2 - y}{y_p - b^w/2} \quad y_p \leq y \leq b^w/2$$

and for the case of $y_p = -b^w/2$ or $y_p = b^w/2$

$$N_y^W = -P \frac{y + y_p}{b^w} \quad -b^w/2 \leq y \leq b^w/2 \quad (5e)$$

where $I = \left(\frac{1}{2} b^f t^f b^{w2} + \frac{1}{12} b^{w3} t^w \right)$.

Assuming that the top and bottom flanges do not distort (i.e., the displacements are linear in the z direction) and considering compatibility conditions at the flange-web intersections, the buckled displacement field for the web, top and bottom flange panels (Fig. 1) of the I-section are derived:

$$u^W = 0, v^W = 0, w^W = w(x, y) \quad \text{for the web} \quad (6a)$$

$$u^{TF} = u^{TF}(x, z) = -z \frac{dw^{TF}}{dx}, v^{TF} = v^{TF}(x, z) = -z\theta^{TF}, w^{TF} = w^{TF}(x) \quad \text{for the top flange} \quad (6b)$$

$$u^{BF} = u^{BF}(x, z) = -z \frac{dw^{BF}}{dx}, v^{BF} = v^{BF}(x, z) = -z\theta^{BF}, w^{BF} = w^{BF}(x) \quad \text{for the bottom flange} \quad (6c)$$

For lateral buckling of I-section beams, the cross-section of the beam is considered as undistorted. As the web panel is not allowed to distort and remains straight in lateral buckling, the sideways deflection and rotation of the web are coupled. The shape functions of buckling deformation for both the sideways deflection and rotation of the web, which satisfy the cantilever beam boundary conditions, can be selected as exact transcendental function, polynomial function or half of the simply-supported beam function [6, 7]. These three shape functions are all considered in this paper. The exact transcendental functions are

$$\begin{Bmatrix} w \\ \theta \end{Bmatrix} = \begin{Bmatrix} \bar{w} \\ \bar{\theta} \end{Bmatrix} \sum_{m=1,2,3,\dots} \left\{ \sin\left(\frac{\lambda_m x}{L}\right) - \sinh\left(\frac{\lambda_m x}{L}\right) - \beta_m \left[\cos\left(\frac{\lambda_m x}{L}\right) - \cosh\left(\frac{\lambda_m x}{L}\right) \right] \right\} \quad (7a)$$

where

$$\beta_m = \frac{\sinh(\lambda_m) + \sin(\lambda_m)}{\cos(\lambda_m) + \cosh(\lambda_m)} \quad (7b)$$

and λ_m satisfies the following transcendental equation

$$\cos(\lambda_m) \cosh(\lambda_m) - 1 = 0 \quad (7c)$$

with $\lambda_1 = 1.875104$, $\lambda_2 = 4.694091$, $\lambda_3 = 7.854757$, ...

The polynomial functions are defined as

$$\begin{Bmatrix} w \\ \theta \end{Bmatrix} = \begin{Bmatrix} \bar{w} \\ \bar{\theta} \end{Bmatrix} \sum_{m=1,2,3,\dots} \frac{1}{(m+1)(m+2)(m+3)(m+4)} \Gamma_m \left(\frac{x}{L} \right) \quad (8a)$$

where

$$\Gamma_m \left(\frac{x}{L} \right) = \left(\frac{x}{L} \right)^{m+4} - \frac{1}{6} (m+1)(m+3)(m+4) \left(\frac{x}{L} \right)^3 + \frac{1}{2} (m+1)(m+3)(m+4) \left(\frac{x}{L} \right)^2 \quad (8b)$$

The half of simply-supported beam functions are considered as

$$\begin{Bmatrix} w \\ \theta \end{Bmatrix} = \begin{Bmatrix} \bar{w} \\ \bar{\theta} \end{Bmatrix} \sum_{m=1,2,3,\dots} \left\{ 1 - \cos \left[\frac{(2m-1)\pi x}{2L} \right] \right\} \quad (9)$$

The displacements and rotations (referring to Eq. (6)) of panels then become

$$\begin{aligned} w^W &= w + y\theta, & w^{TF} &= w + \frac{b^w}{2}\theta, & w^{BF} &= w - \frac{b^w}{2}\theta \\ \theta^{TF} &= \theta^{BF} = \theta \end{aligned} \quad (10)$$

By applying the Rayleigh-Ritz method and solving for the eigenvalues of the potential energy equilibrium equation, the lateral buckling load, P_{cr} , for a free-end point load applied at the centroid of the cross-section is obtained. For different assumed buckling shape functions, the explicit equations of critical buckling load are given as follows:

The critical buckling load based on exact transcendental shape function is:

$$P_{cr} = \Psi_1 \cdot \left\{ b^w L \Psi_2 + (\sqrt{\Psi_3 + \Psi_4 + \Psi_5 + \Psi_6 + \Psi_7}) / b^w \right\} \quad (11)$$

where

$$\begin{aligned} \Psi_1 &= (6b^f + b^w) / [2L^3 \cdot (76.5b^{f^2} - 6.96b^f b^w + 0.16b^{w^2})] \\ \Psi_2 &= (123b^f - 5.6b^w) D_{16} \\ \Psi_3 &= a_{11} b^{f^3} (279.5b^{f^2} - 25.5b^f b^w + 0.6b^{w^2}) \\ \Psi_4 &= 6707.5b^{f^5} b^{w^3} d_{11} D_{11} - 610.8b^{f^4} b^{w^4} d_{11} D_{11} + b^{f^3} b^{w^3} D_{11} (13.9b^{w^2} d_{11} + 30261L^2 d_{66}) \\ \Psi_5 &= b^f b^{w^5} (62.7L^2 d_{66} D_{11} - 305.4b^{w^2} D_{11}^2 - 1377.4L^2 D_{16}^2 - 5511L^2 D_{11} D_{66}) \\ \Psi_6 &= b^{w^6} (7b^{w^2} D_{11}^2 + 31.4L^2 D_{16}^2 + 125.5L^2 D_{11} D_{66}) \\ \Psi_7 &= a_{11} b^{f^3} b^{w^2} (1118b^{f^5} d_{11} - 101.8b^{f^4} b^w d_{11} + 2.3b^{f^3} b^{w^2} d_{11} + 5043.5b^{f^3} L^2 d_{66} \\ &\quad + 4.64b^{w^5} D_{11} + 20.9b^{w^3} L^2 D_{66}) \\ \Psi_8 &= a_{11} b^{f^4} b^{w^3} [b^w (-203.6b^{w^2} D_{11} + 10.5L^2 d_{66} - 918.5L^2 D_{66}) \\ &\quad + b^f (2235.8b^{w^2} D_{11} - 459.5L^2 d_{66} + 10087L^2 D_{66})] \end{aligned}$$

The critical buckling load based on fifth-order polynomial function is:

$$P_{cr} = \Psi_1 \cdot \left\{ 945Lb^w D_{16} + \sqrt{17424a_{11}^2 b^{f^2} b^{w^2} + 176a_{11} b^{f^3} \Psi_2 + 3b^w (\Psi_3 + \Psi_4)} \right\} \quad (12)$$

where

$$\Psi_1 = \frac{30(6b^f + b^w)}{7L^3(5160b^f - 229b^w)}$$

$$\Psi_2 = 396b^{f^3} d_{11} + 1763L^2 b^f d_{66} + 792b^{w^3} D_{11} + 3526L^2 b^w D_{66}$$

$$\Psi_3 = 139392b^{f^3} d_{11} D_{11} + 620576L^2 b^f d_{66} D_{11}$$

$$\Psi_4 = 297675L^2 D_{16}^2 + 704D_{11}(99b^{w^2} D_{11} + 1763L^2 D_{66})$$

The critical buckling load based on half simply-supported beam function is:

$$P_{cr} = \Psi_1 \cdot \left\{ 96Lb^w D_{16} + \sqrt{\pi^4 a_{11}^2 b^{f^6} b^{w^2} + 4\pi^2 a_{11} b^{f^3} \Psi_2 + 12b^w \Psi_2} \right\} \quad (13)$$

where

$$\Psi_1 = \frac{\pi^2(6b^f + b^w)}{24L^3(35.22b^f - 2.13b^w)}$$

$$\Psi_2 = \pi^2 b^{f^3} d_{11} + 48L^2 b^f d_{66} + 2\pi^2 b^{w^3} D_{11} + 96L^2 b^w D_{66}$$

$$\Psi_3 = 2\pi^4 b^{f^3} d_{11} D_{11} + 96\pi^2 L^2 b^f d_{66} D_{11} + b^w [\pi^4 b^{w^2} D_{11}^2 + 192L^2(4D_{16}^2 + \pi^2 D_{11} D_{66})]$$

and in Eqs. (11) to (13), the following material parameters are defined as:

$$a_{11} = 1/\alpha_{11}, a_{66} = 1/\alpha_{66}, d_{11} = 1/\delta_{11}, d_{66} = 1/\delta_{66}$$

Experimental Evaluations

In this study, four geometries of FRP I-beams, which were manufactured by the pultrusion process and provided by Creative Pultrusions, Inc., Alum Bank, PA, were tested to evaluate their lateral buckling responses. The four I-sections consisting of (1) I4×8×3/8 in. (I4x8); (2) I3×6×3/8 in. (I3x6); (3) WF4×4×1/4 in. (WF4x4); and (4) WF6×6×3/8 in. (WF6x6) were made of E-glass fibers and polyester resins. Based on the lay-up information provided by the manufacturer and a micro/macromechanics approach [8], the panel material properties of the FRP I-beams are obtained and used in explicit solutions (Eqs. (11) to (13)). The clamped-end of the beams was achieved using two steel angles attached to a vertical steel column. Using a loading platform, the loads were initially applied by sequentially adding steel angle plates of 111.2 N (25.0 lbs), and as the critical loads were being reached, incremental weights of 22.2 N (5.0 lbs) were added until the beam buckled. The tip load was applied through a chain attached at the centroid of the cross section. Two LVDTs and one level were used to monitor the rotation of the cross section, and the sudden sideways movement of the beam was directly observed in the experiment. The buckled shape of a representative I-beam at a span length of 365.8 cm (12.0 ft.) is shown in Figure 2, and the corresponding critical loads for various structural shapes were obtained by summing the weights added during the experiments. Varying span lengths from 182.9 cm (6.0 ft.) to 396.2 cm (13.0 ft.), two beam samples per geometry were evaluated, and an averaged value for each pair of beam samples was considered as the experimental critical load.



Figure 2. Buckled I3x6 beam

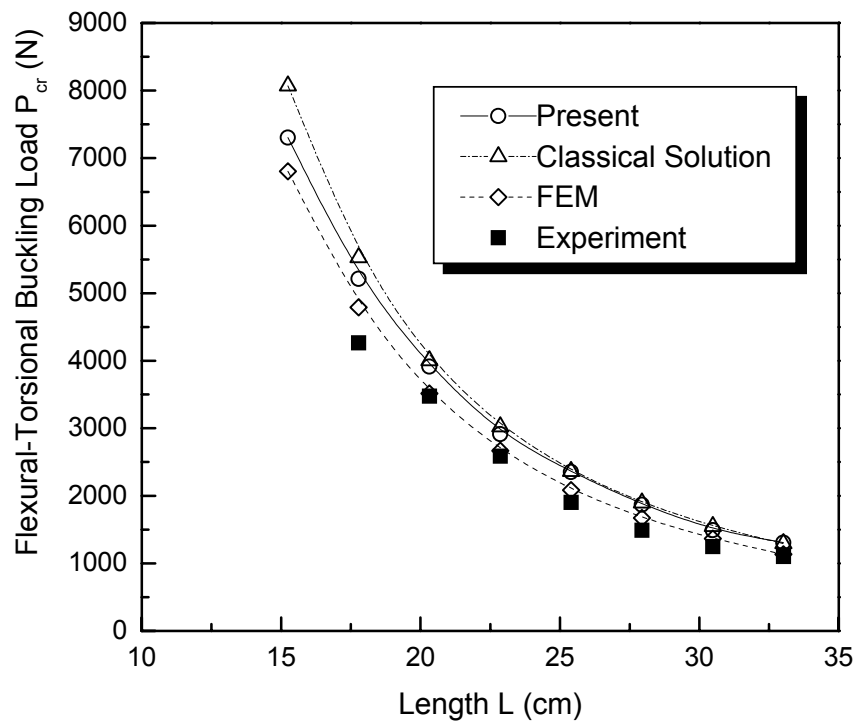


Figure 3. Lateral buckling load of I3x6 beam

Results and Discussion

To verify the accuracy of the proposed analytical approach, the four experimentally tested FRP I-beam sections are considered (i.e., I4×8, I3×6, WF4×4 and WF6×6). The analytical solutions and experimental results are also compared with classical approach based on Vlasov theory [9] and finite element method (FEM). The commercial finite element program ANSYS is employed for modeling of the FRP beams using Mindlin eight-node isoparametric layered shell elements (SHELL99). The comparisons of critical buckling loads among analytical solution using the exact transcendental shape function, the classical Vlasov theory [9], experimental data and finite element results are given in Table 1 for span lengths of $L = 304.8 \text{ cm}$ (10.0 ft.) and $L = 365.8 \text{ cm}$ (12.0 ft.), and the present analytical solution shows a good agreement with FEM results and experimental data. The critical buckling loads versus the lengths (L) for the beam I3×6 is shown in Figure 3, and it indicates that the present analytical predictions for exact transcendental shape function are slightly higher than the FEM results but close to experimental values and lower than the classical solution using Vlasov theory [9]. As expected, the critical load decreases as the span length increases and lateral buckling becomes more prominent. The present predictions show a good agreement with FEM results and experimental data for long beam spans, while for shorter span-lengths the buckling mode is more prone to lateral-distortional instability which is not considered in the present study.

Table 1. Comparisons for Lateral Buckling Loads of I-Beams

Length L (cm)	Section	Analytical solution P_{cr} (N)	Classical solution P_{cr} (N)	Finite element P_{cr} (N)	Experimental data P_{cr} (N)
304.8	I4×8	4,765	5,201	4,503	4,010
	I3×6	2,338	2,360	2,174	2,058
	WF4×4	1,498	1,783	1,436	1,476
	WF6×6	8,526	10,860	8,624	—
365.8	I4×8	3,192	3,321	2,956	2,943
	I3×6	1,494	1,547	1,365	1,356
	WF4×4	1,014	1,151	933	920
	WF6×6	5,614	6,428	5,774	5,476

Note: Analytical solution based on exact transcendental shape function; Classical solution based on the Vlasov theory [9].

Effect of Mode Shape Function

The accuracy and convergence of different assumed buckling shape functions (i.e., exact transcendental shape function, fifth-order polynomial function and half simply-supported beam function) are also investigated. The critical buckling loads using the three types of buckling shape functions are compared with the FEM results for the span length of $L = 304.8 \text{ cm}$ (10.0 ft.) and $L = 365.8 \text{ cm}$ (12.0 ft.) and for varying span lengths (see Fig. 4 for I3×6 beam). As shown in Fig. 4, the analytical solutions using exact transcendental shape function and fifth-order polynomial function show relatively good correlations with FEM results; whereas the solution with half simply-supported beam function which is commonly used in the cantilever beam modeling demonstrates a large discrepancy. Therefore, the exact transcendental function and fifth-order polynomial function should be selected in the lateral buckling simulation.

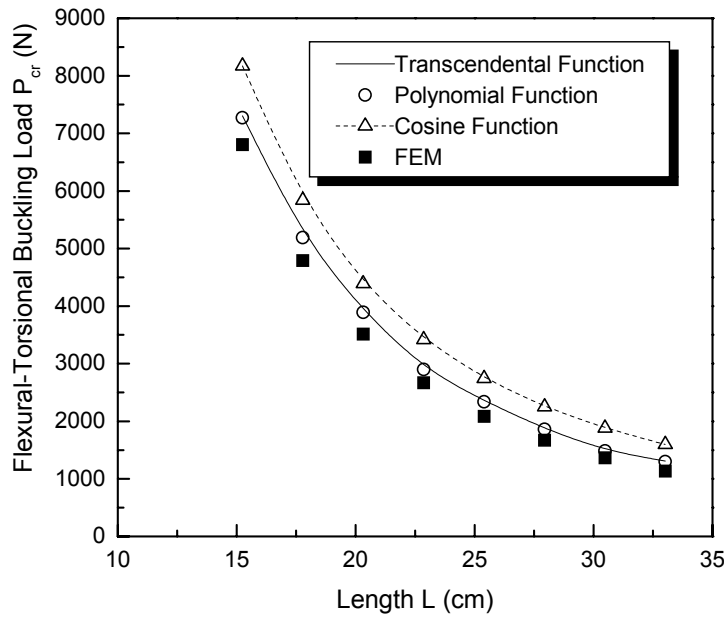


Figure 4. Comparison of lateral buckling for I3×6 using different assumed buckling shape functions

Effect of Load Locations

To account for the location of the applied load along the vertical direction of the beam tip cross section, the transverse stress resultant on the web panel is represented in Eqs. (5d) and (5e), and the analytical solutions can be formulated to obtain the critical buckling loads at any location along the web at the load-tip cross section. The comparisons of critical buckling loads among three locations (centroid, top and bottom) are shown in Fig. 5 for the beam I3x6, and they demonstrate that as the load height increases, the beam is more vulnerable to buckling.

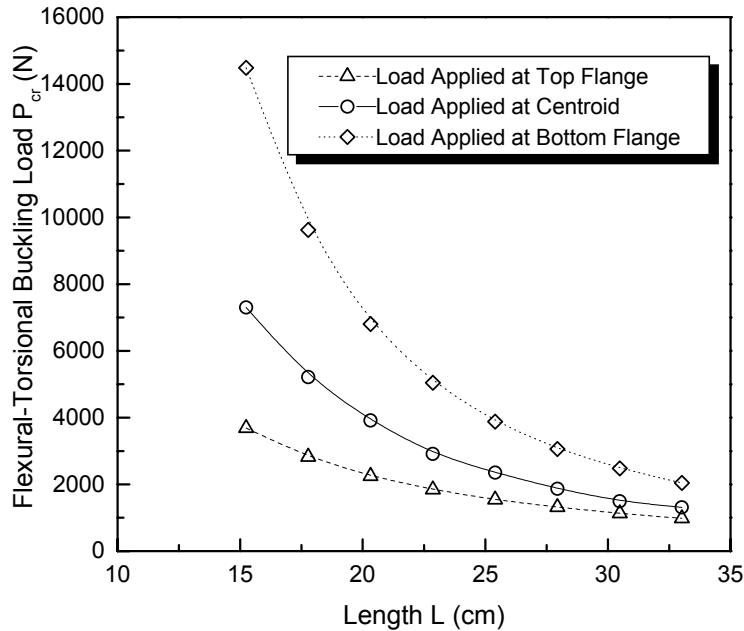


Figure 5. Lateral buckling load for I3×6 beam at different applied load positions

Effect of Fiber Architecture and Fiber Volume Fraction

To investigate the effect of fiber angle orientation on lateral buckling behavior, the original stitched $\pm 45^\circ$ angle layers in the laminated panels of WF4x4 were substituted by $(\pm\theta)$ layers with θ as a design variable. The critical buckling load with respect to ply angle (θ) at fiber volume fraction of 50% is shown in Fig. 6, where a maximum critical buckling load can be observed at $\theta = 30^\circ$ for the tip load applied at the centroid of the cross-section. Similarly, the effect of fiber volume fraction on lateral buckling behavior is studied, and the lateral buckling load versus fiber volume fraction is shown in Fig. 7. As anticipated, the fiber volume fraction is of significant importance for improving the buckling resistance.

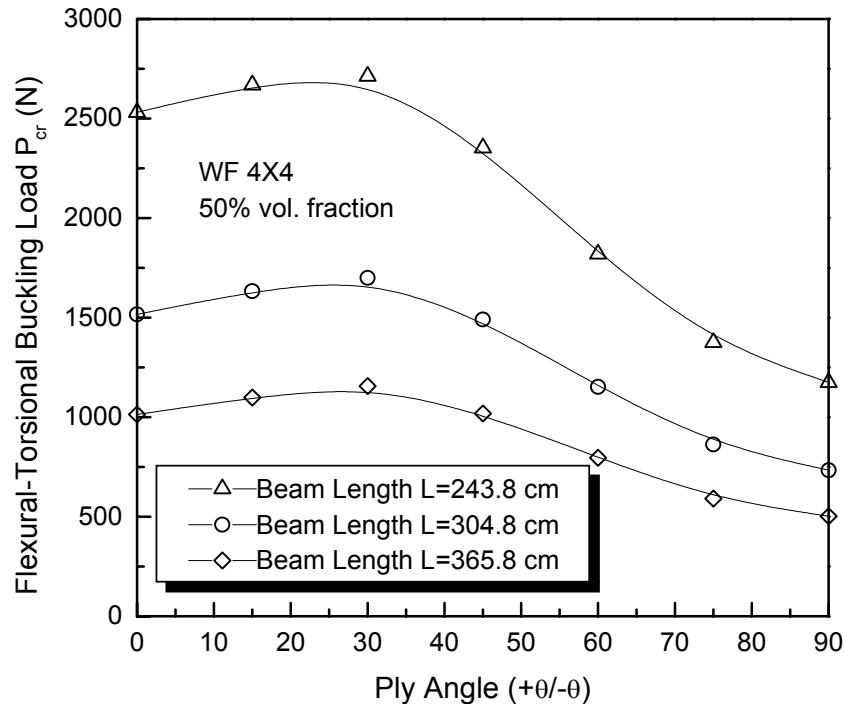


Figure 6. Influence of lamination angle ($+\theta/-\theta$) on Flexure-torsional buckling of WF 4x4 beam

Conclusions

In this paper, a combined analytical and experimental study is presented to study the lateral buckling behavior of pultruded Fiber-Reinforced Plastic (FRP) composite cantilever I-beams. The total potential energy based on nonlinear plate theory is derived, and shear effects and beam bending-twisting coupling are accounted for in the analysis. Three different types of buckling mode shape functions, namely transcendental function, polynomial function, and half simply-supported beam function, which all satisfy the cantilever beam boundary conditions, are used to obtain the analytical solutions and explicit prediction formulas. An experimental study of four different geometries of FRP cantilever I-beams is performed, and the critical lateral buckling loads for different span lengths are obtained. A good agreement among the proposed analytical solutions, experimental testing, and finite-element method is obtained. The study on effect of buckling mode shape functions indicates that the approximations by exact transcendental function and polynomial function compare well with FEM results and may be more applicable for the buckling modeling of cantilever beam configuration. A

parametric study on the effects of load location through the height of the cross section, fiber orientation and fiber volume fraction on buckling behavior is also presented. The explicit and experimentally-validated analytical formulas for the lateral buckling prediction can be effectively used to design and characterize the buckling behavior of FRP structural shapes.

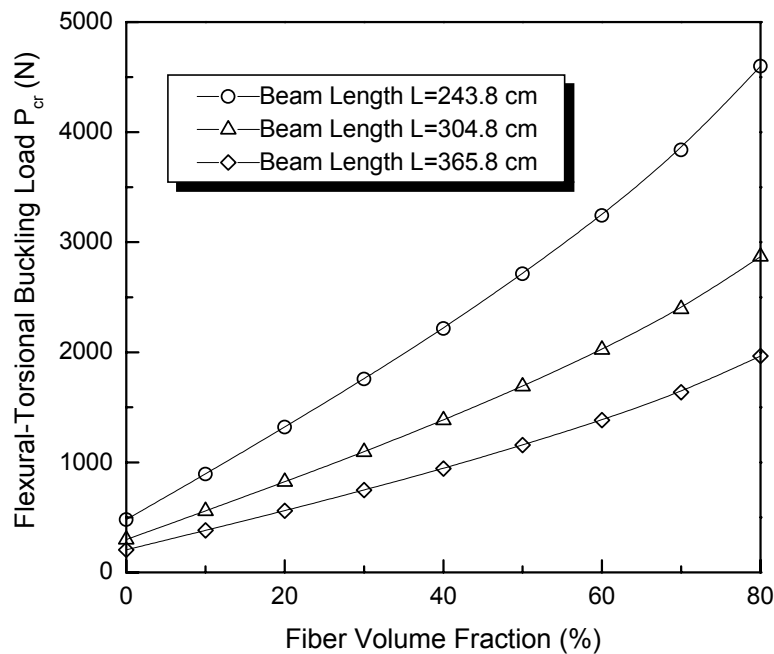


Figure 7. Influence of fiber volume fraction on lateral buckling of WF4×4 beam

References

1. Barbero, E. J., and Raftoyiannis, I. G. (1994). Lateral and distortional buckling of pultruded I-beams, *Composite Structures*, 27(3), 261-268.
2. Davalos, J. F., Qiao, P. Z., and Salim, H. A. (1997). Flexure-torsional buckling of pultruded fiber reinforced plastic composite I-beams: experimental and analytical evaluations, *Composite Structures*, 38(1-4), 241-250.
3. Davalos, J. F., and Qiao, P. Z. (1997). Analytical and experimental study of lateral and distortional buckling of FRP wide-flange beams, *J. Composites for Construction*, 1(4), 150-159.
4. Qiao, P. Z., Davalos, J. F., Barbero, E. J., Troutman, D. (1999). Equations Facilitate Composite Designs, *Modern Plastics*, 76(11): 77-80.
5. Qiao, P. Z., Zou, G. P., and Davalos, J. F. (2002). Flexural-torsional buckling of fiber-reinforced plastic composite cantilever I-beams, submitted to *Engineering Structures*.
6. Elishakoff, I. and Guede, Z. (2001). Novel closed-form solution in buckling of inhomogeneous columns under distributed variable loading, *Chaos Solutions and Fractals*, 12, 1075-1089.
7. Zou, G. P. (1998). An exact symplectic geometry solution for the static and dynamic analysis of Reissner plates, *Comput. Methods Appl. Mech. Engrg.*, 156, 171-178.
8. Davalos, J. F., Salim, H. A., Qiao, P. Z., Lopez-Anido, R., and Barbero, E. J. (1996). Analysis and design of pultruded FRP shapes under bending, *Composites Part B: Engrg. J.*, 27B, (3/4), 295-305.
9. Pandey, M. D., Kabir, M. Z., and Sherbourne, A. N. (1995). Flexural-torsional stability of thin-walled composite I-section beams, *Composites Engineering*, 5(3), 321-342.